www.project-foci.eu

Co-funded by the European Union

UK Research and Innovation

Horizon Europe

(HORIZON-CL5-2021-D1-01)

Non-CO2 Forcers and their Climate, Weather, Air Quality and Health Impacts

FOCI

Deliverable 3.2

Model improvements on aerosol optical properties

Grant Agreement No.	101056783	
Project acronym	FOCI	
Project full title	Non-CO2 Forcers and their Climate, Weather, Air Quality and Health Impacts	
Call	HORIZON-CL5-2021-D1-01	
Deliverable name	D.3.2 Model improvements on aerosol optical properties	
WP contributing to the deliverable	WP3	
Task producing the deliverable	Task 3.2	
Type	X	Report
		Prototype
		Demonstrator
		Other: Data
Dissemination level	X	Public
		Sensitive
		UE/EU-Restricted
Due date of deliverable	Month 30	
Actual submission date	Month 36	
Lead beneficiary	MPIC	
Author(s)	Sergey Gromov (MPI-C), Andrea Pozzer (MPI-C), María Gonçalves-Ageitos (BSC), Vincenzo Obiso (BSC), Marios Chatziparaschos (BSC), Montserrat Costa Surós (BSC), Oriol Jorba (BSC), Twan van Noije (KNMI), Lianghai Wu (KNMI), Philippe Le Sager (KNMI), Vincent Huijnen (KNMI), Tommi Bergman (FMI), Harri Kokkola (FMI), Anton Laakso (FMI)	
Other Contributor(s)		
Reviewer(s)	Sandro Finardi (ARIANET)	
Keywords	FOCI, global model, development	

ACKNOWLEDGEMENTS

This project has been co-funded by the European Union with funding from the European Union's Horizon Europe research and innovation programme under grant agreement No. 101056783 and from UKRI under the UK Government's Horizon Europe Guarantee (UKRI Reference Numbers: 10040465, 10053814 and 10050799).

Version	Date	Modified by	Comments
1.0	1 Aug 2025	Sergey Gromov	First draft written
1.1	18 Aug 2025	Andrea Pozzer	Finalized for internal review
1.2	28 Aug 2025	Andrea Pozzer	Revised based on the review comments

	Name	Date
Verification Final Draft by WP leaders	Oriol Jorba (BSC) Twan van Noije (KNMI)	28 August 2025
Check before upload by project Coordinator	Tomáš Halenka	29 August 2025

TABLE OF CONTENTS

EXECUTIVE SUMMARY

This document is the deliverable “D3.2: Model improvements on aerosols optical properties” for the European Union project “FOCI: Non-CO2 Forcers and their Climate, Weather, Air Quality and Health Impacts” (hereinafter also referred to as FOCI, project reference: 101056783).

The report describes the improvement of model simulation of aerosols composition and their optical properties, both in EC-Earth and EMAC. In EMAC, particular attention was given to improving the representation of carbonaceous aerosols, allowing a clearer distinction between strongly absorbing species (such as black and brown carbon) and more scattering types (like secondary organic aerosols). In EC-Earth4, updates focused on the optical treatment of mineral dust, incorporating dependencies on dust composition. Notably, all revised optical properties now include full spectral (wavelength-dependent) resolution.

CONTRIBUTION TO THE FOCI OBJECTIVES

This deliverable is on the Earth system model development activities in WP3. The work described in this report contributes to the project objective O4:

> "To improve and evaluate state-of-the-art global ESMs (WP3) and regional climate and atmospheric composition models (RCMs) (WP4), targeting specific critical processes with the largest uncertainties (WP6) for improving future next generation climate projections"

1. INTRODUCTION

This report presents advancements in the representation of aerosol radiative processes within two Earth System Models (ESMs): EC-Earth4 and EMAC. EC-Earth4 is the forthcoming version of the EC-Earth model, a European community ESM developed by the EC-Earth consortium (https://ec-earth.org/consortium/), currently under development in preparation for participation in the Coupled Model Intercomparison Project Phase 7 (CMIP7). Its atmospheric component is based on the OpenIFS model developed by the European Centre for Medium-Range Weather Forecasts (ECMWF). EMAC (ECHAM5/MESSy Atmospheric Chemistry) is a modular ESM developed through a multi-institutional effort. It employs the Modular Earth Submodel System (MESSy) framework to integrate various scientific codes, enabling detailed studies of atmospheric chemistry and its interactions with the climate system. Within both EC-Earth4 and EMAC, aerosol optical properties have been newly defined or refined. In EMAC, particular attention was given to improving the representation of carbonaceous aerosols, allowing a clearer distinction between strongly absorbing species (such as black and brown carbon) and more scattering types (like secondary organic aerosols). In EC-Earth4, updates focused on the optical treatment of mineral dust, incorporating dependencies on dust composition. Notably, all revised optical properties now include full spectral (wavelength-dependent) resolution. While initial evaluations of these developments have been conducted, a more detailed analysis is planned under Task 3.4. This report serves to document the implemented model updates and their scientific basis.

2. DESCRIPTION OF MODEL IMPROVEMENT

2.1 EMAC model

The Modular Earth Submodel System (MESSy) (Jöckel et al., 2005) provides a framework for constructing comprehensive Earth System Models (ESMs) using process-based modules, known as submodels. MESSy is designed with standardized interfaces to integrate various components, a consistent coding structure, and a suite of submodels developed according to these principles. The MESSy framework is organized into four distinct layers: (i) Basemodel Layer (BML) consisting of a central clock and run-time control but typically includes a general circulation model (GCM) or a box model; (ii) Basemodel Interface Layer (BMIL) including the MESSy infrastructure within the basemodel and serves as a communication hub between the basemodel and the submodels; (iii) Submodel Interface Layer (SMIL): Acts as the connection between specific processes and the BMIL infrastructure; and (iv) Submodel Core Layer (SMCL): Contains the implementation of Earth System processes or diagnostic tools, independent of the basemodel. It operates using data provided via the SMIL and supplies data back to other submodels and/or the basemodel. A comprehensive list of available submodels in MESSy can be found at www.messy-interface.org. Thanks to the continuous development of chemistry-based submodels, MESSy has proven to be a flexible tool for implementing Chemistry–Climate Models (CCMs). CCMs are sophisticated computational tools designed to simulate and analyse the complex interactions between atmospheric chemistry and climate variables. They allow for the isolation and detailed study of different climate system processes and can simulate potential future climate scenarios, assessing how various processes respond to perturbations induced by rapid climate change. This, in turn, contributes to the development of adaptive responses and mitigation strategies. The most widely used implementation of MESSy as a CCM is with the European Centre for Medium-Range Weather Forecasts – Hamburg v5 (ECHAM5) basemodel (Roeckner et al., 2006), referred to as EMAC (ECHAM5/MESSy for Atmospheric Chemistry). EMAC was among the first community models capable of simulating the chemistry and dynamics of the stratosphere and troposphere as a unified system within global models (Jöckel et al., 2006).

2.1.1 Development of new aerosol optical properties

Within the current project objective, the new MESSy submodel for Aerosol Optical Properties (AOP) was developed to offer a substantially greater flexibility than the previously utilised submodel AEROPT. AOP computes particles mode-averaged refractive indices based on chemical composition and derives key optical properties like extinction, single scattering albedo and asymmetry factor, using pre-calculated Mie parameters. The total optical properties for each model grid cell are then obtained by weighting the contributions of individual modes according to their number distributions, followed by interpolation or calculation to the target wavelengths.

Compared to the earlier hard-coded implementation, AOP allows for a flexible number of aerosol size modes and offers greater adaptability in handling aerosol optical properties across varying chemical compositions, allowing pre-calculating necessary properties during model simulation. While AEROPT already distinguished between bulk organic matter, dust, soot, sea salt, water-soluble species and sulfuric acid, in AOP we extended this set by introducing explicit optical properties for (volcanic) ash and speciated organic carbon (OC), including Secondary Organic Aerosol (SOA), Brown Carbon (BrC), and residual primary organic carbon. While the optical properties implementation has been extended to additional aerosol components, no changes were made on the capabilities of the model to simulate atmospheric composition.

Implementation of AOP allowed to achieve a more accurate representation of atmospheric aerosols throughout the atmosphere in a new "whole-atmosphere" (WA) EMAC setup which more consistently represents diverse atmospheric domains spanning from the surface to the upper stratosphere. Previously, model setups were specifically tailored for accurate representation of either stratospheric or tropospheric compositions, which resulted in poor performance of either in other domains, a common shortcoming of EMAC in the upper troposphere/lowermost stratosphere regions. Using AOP, we have introduced the extended 5-modes scheme with the additional "small course" mode bridging the accumulation and coarse modes (listed in Table 1). A preliminary evaluation of the new scheme confirms better representation of aerosol growth processes and lifetimes specifically in the upper troposphere and lowermost stratosphere. The calculation of optical properties in the new scheme was carried out using the new AOP submodel.

Table 1. Modal size distribution in the new whole atmosphere (WA) setup compared to the earlier separate tropospheric (TR) and stratospheric (ST) setups. The "small coarse" mode is devised to bridge the accumulation and coarse modes.

Setup		Diameter range [nm] (modal width, σ)				
	Mode	Nucleation	Aitken	Accumulation	Small Coarse	Coarse
TR		1–12 (1.59)	12–120 (1.59)	120–1400 (1.59)	–	>1400 (2.0)
ST		1–12 (1.59)	12–140 (1.59)	140–3200 (1.49)	–	>3200 (1.7)
WA		1–12 (1.59)	12–120 (1.59)	120–800 (1.4)	800–3200 (1.25)	>3200 (1.7)

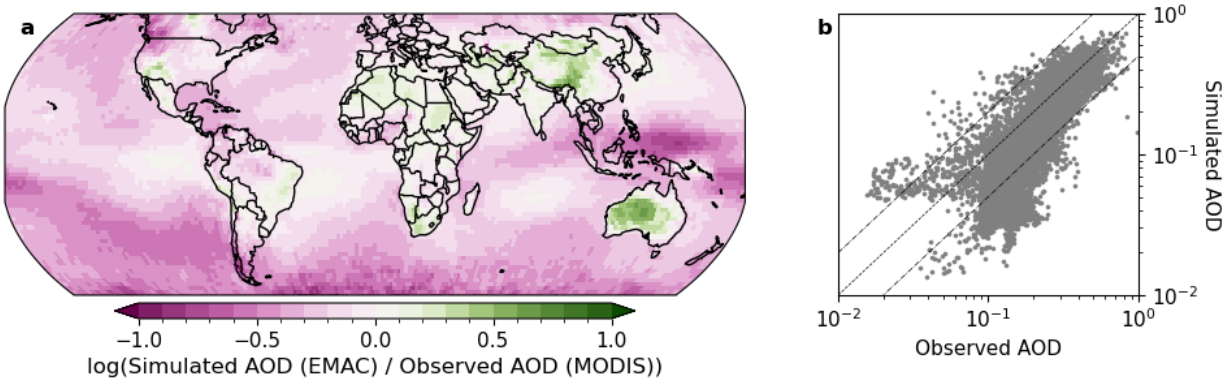

Figure 1. Comparison of annually averaged (year 2017) simulated column Aerosol Optical Depth (AOD) from EMAC (WA setup) with MODIS observations at 550 nm. (a) Global map of the logarithmic ratio of simulated to observed AOD; green indicates overestimation by the model, pink indicates underestimation. (b) Scatter plot comparing simulated and observed AOD globally. Each dot represents one model grid box. The central dotted line indicates 1:1 agreement between observations and simulations, while the surrounding dashed lines represent overestimation and underestimation by a factor of two.

The new EMAC WA model setup was extensively evaluated using ground-based (GHOST database prepared in FOCI project, EPA, EEA AQ, EMEP data, etc.), aircraft (ATom, EMeRGe, CAFE-Africa/Brazil/Pacific, StratoClim and ACCLIP campaigns) and satellite observations (OSIRIS, CALIOP, SAGE-III, GloSSAC and MODIS). Figure 1 shows the evaluation of the EMAC-simulated column Aerosol Optical Depth (AOD) and observations from the MODIS instrument. Higher AOD values, particularly those observed in polluted regions, are well reproduced in the simulations (typically within a factor of two). Some overestimations over desert areas are present, possibly due to the coarse assumption on dust optical properties in this model simulation. On the other side, the model tends to underestimate AOD over the remote oceans likely attributed to (i) misrepresentation of sea salt aerosol number densities, (ii) lack of aerosols formation (nucleation) from precursors emitted by ocean and typical for marine environment (e.g. from halogen or sulfur-containing gases).

Stratospheric AOD and extinction simulated in the three EMAC evaluation setups were compared with satellite observations derived from GloSSAC observations (shown in Figure 2). The Global Space-based Stratospheric Aerosol Climatology, or GloSSAC, is a 38-year climatology of stratospheric aerosol properties focused on extinction coefficient measurements by the Stratospheric Aerosol and Gas Experiment (SAGE) series of instruments through mid-2005 and on the Optical Spectrograph and InfraRed Imager System (OSIRIS) and the Cloud-Aerosol Lidar and Infrared Pathfinder Satellite Observation (CALIPSO) data thereafter. Data from other space instruments and from ground-based, air and balloon borne instruments to fill in key gaps in the data set. The end result is a global and gap-free data set focused on aerosol extinction coefficient at 525 and 1020 nm. The selected period for the model evaluation (from January 2016 to December 2018) was relatively volcanically quiescent (Schallock et al., 2023), mostly representing background stratospheric conditions. In general, the simulations with the stratospheric (ST)/tropospheric (TR) setups produce highest/lowest AOD values, respectively, which is explained by the differences in used size modes distribution (see Table 1 above). In the TR setup, aerosols rapidly grow into the coarse mode and subsequently quicker sediment from the stratosphere. In contrast, the accumulation mode in the ST setup has wider mode boundaries and narrower sigma of the log-normal distribution, which limits growth into the coarse mode, resulting in a more realistic stratospheric size distribution. Introduction of the intermediate mode in the WA setup buffers this effect: while particles still grow into the small coarse modes, sedimentation is reduced compared to that in the TR setup, although the stratospheric lifetime of the particles slightly decreases compared to that in the ST setup. It must be stressed that the difference in optical absorption between the different setups stems also from another effect. Particles

with a diameter similar to the incident radiation scatter most efficiently according to Mie scattering, depending on aerosol composition (e.g. Bohren and Huffman, 1998). As a result, both setups (WA and ST) show much better agreement at 1020 nm and matching the observations, due to the presence of a larger coarse mode (above 3200 nm) compared to the TR configuration (see Table 1) The newly adjusted size distribution, however, exhibits a minimum around 500 nm due to the mode boundary at 800 nm, and is a computational effect. While this could be corrected by the addition of a further aerosol mode, the resulting computational cost would increase significantly. We therefore decide to maintain the current set-up, being an optimal compromise between computational costs and simulation accuracy.

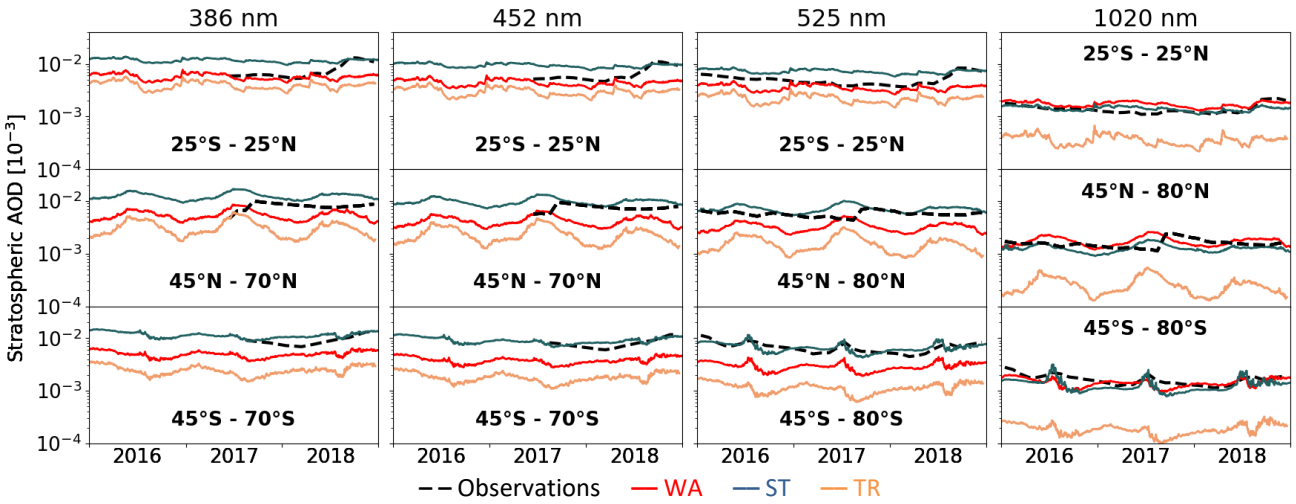

Figure 2. Time series of simulated stratospheric AOD in the three EMAC setups compared to observations from the GloSSAC database at the four GloSSAC wavelengths (left to right), in the tropics (top), NH higher latitudes (middle), and SH higher latitudes (bottom).

2.1.2 Updated OC/BC and introduced BrC optical properties

A further development of the aerosol physics representation in EMAC was accomplished in FOCI through revisiting the to date used optical properties of organic and black carbon (BC and OC, respectively) following the introduction of new brown carbon (BrC) species, a distinguishing separate class of organic aerosols differing from organic aerosols (OA) in higher efficiency in absorbing UV and visible radiation. BrC is a wide class of aerosol species whose reported optical properties span from near-dark (close to BC) to transparent/reflective (close to OC) and are potent in their impact on Earth's climate radiative forcing (RF). To date, uncertainties about BrC contribution to the RF are larger compared to that of BC/OC, trace gases and other factors (IPCC, 2023) which is to a considerable extent due to current Earth System Models (ESMs) lacking sufficient representation of BrC. Since no consistent unified classification and framework for BrC implementation in ESMs has been developed yet, we have reviewed options and strategy of BrC implementation in the recent EMAC/MOM version including the state-of-the-art gas- and aerosol-phase organics representation (Pozzer et al., 2022).

Although several reported BrC optical properties is available from ambient measurements, these represent various mixing states of BrC at different ages (e.g. degree of photochemical processing) and are generally not suitable for a process-based (submodel) implementation. However, there are a few controlled lab experiments (e.g. Alexander et al., 2008; Hoffer et al., 2017) whose data could be projected onto two principal kinds of BrC, viz. fresh and aged, implemented in EMAC. The former, darker "fresh" tarballs originate from primary OA sources (mostly biomass burning) and resemble reflectivity of OC previously implemented in EMAC, however

with more efficient absorption in the shortwave (SW) range. The latter, lighter BrC represent secondary OA formed from gas-phase precursors and bleached tarballs that underwent photochemical. Fresh/aged BrC generally resemble OC/BC absorption efficiencies in SW than originally used in EMAC. Implementation of source-specific emission fractions of BrC species as well as aging parameterisation (conversion of fresh to aged species) allow simulating variable mixing states of BrC. Some further details on the BrC implementation in EMAC were reported during intermediary presentation of this FOCI activity (Gromov et al., 2025).

Following the introduction of BrC in EMAC (in AEROPT and subsequently AOP submodels, see Sect. 2.1.1 above), optical properties of OC and BC had to be reviewed, as their profiles implicitly included an assumed fraction of (to date not implemented) BrC inherited from optical properties databases (e.g. OPAC). Recent literature recommendations for OC and BC optical properties suggest much weaker absorption of OC in the SW and greater reflectivity in the longwave (LW) ranges. Such is the case for more recent OC optical properties profiles adapted from another Earth System Model (the Community Earth System Model, CESM2), from which we obtained the LW and SW band-by-band cloud radiative kernel (Huang et al., 2019). Regarding the BC, its absorption was updated to be close to unity in the entire simulated wavelength range (as BC absorbs virtually at any wavelength), thus correcting the earlier lower absorption in the LW range. Original, updated and newly introduced optical properties of OC, BC and BrC species in EMAC are presented in Figure 3.

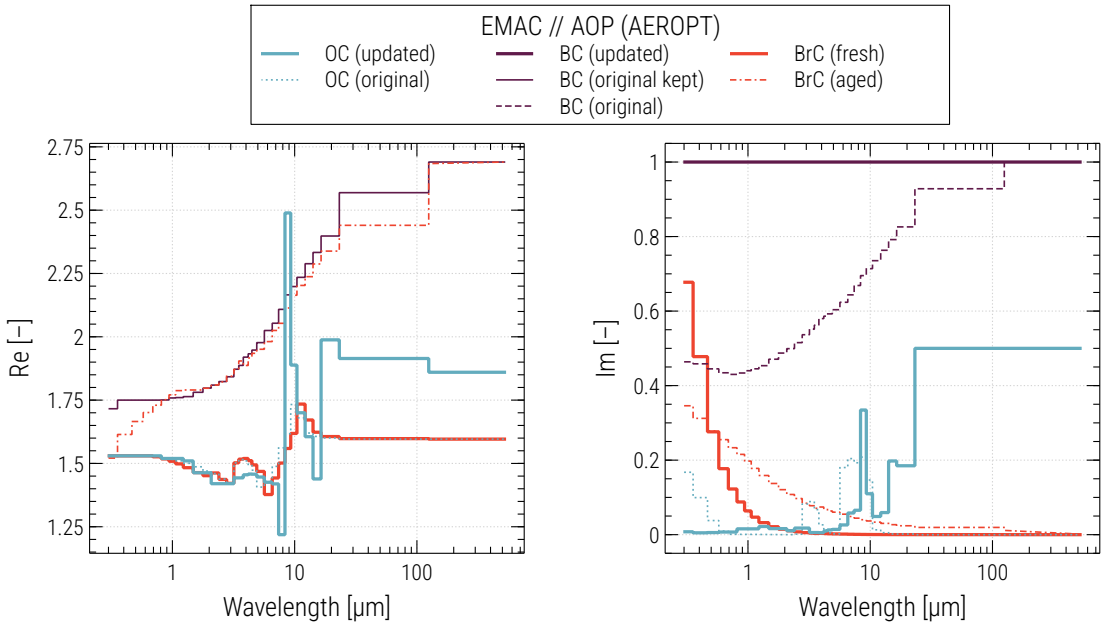

Figure 3. Original, updated and newly introduced optical properties of carbonaceous aerosol species in EMAC. Left and right panels show the real (refractive index) and imaginary (absorption coefficient) parts of species' refractive indices, respectively. New properties are implemented in submodels (both earlier used AEROPT and newly developed AOP) simulating optical properties of aerosols in EMAC.

Several evaluation simulations were carried out with the EMAC in order to estimate the sensitivity of radiative forcing (RF, instantaneous) to the improved representation of aerosol optical properties introduced. Using the comprehensive setup for simulations developed in the project for the MOM model configuration (Pozzer et al.2022), we have applied black carbon (BC)-like properties to the bulk of primary OA represented in the model. The reference and sensitivity simulations were integrated in medium resolution (T63L31ECMWF, ~1.88° horizontal grid size, up to 10 hPA) due to computationally very intensive chemistry and detailed aerosol microphysics (with 7 modes and full gas-aerosol equilibrium) implementation, with specified tropospheric dynamics for 2009−2010 and no chemical/aerosol feedback on dynamics. The resulting sensitivities indicate a

substantial sensitivity of the RF to the BrC properties, with increases up to +(0.452–0.466) W/m^2 (from a reference value of +(6.04±0.71) W/m^2) in terms of net top-of-atmosphere annual averages. This exceeds the current RF estimates for OC and BrC (about −0.2 and +0.15 W/m^2, respectively, figs. from IPCC, 2023, Chapter 6) by a factor two or more and justifies BrC speciation development further performed within the project.

A subsequent set of evaluation simulations was performed with the EMAC FOCI setup tailored for longer-term simulations used in other (cross-cutting) project activities. The main difference to the setup described above is the use of computationally efficient (reduced) organic chemistry scheme which allowed integrating the 2000–2020 period in order to obtain sufficient statistics for projections of the RF sensitivity to the changes in OA optical properties. No BrC simulation was included. The latter were separately updated and simulated in individual sensitivity simulations. The obtained sensitivities (shown in Figure 4) exhibit about 4 times larger instantaneous RF responses to OC properties changes compared to that for BC. For OC, largest changes are typically co-located with the regions of SOA production and biogenic POA emission sources. For BC, co-location occurs only with POA emissions. The resulting sensitivities are typically of opposite sign and about factor 4/5 larger at the top of simulated atmosphere compared to surface, which is attributed to changes backscatter and greater LW absorption. The opposite sign is due to the fact that an increase (or decrease) absorption in the atmosphere does increase(decrease) the net radiation at the top of the atmosphere, while simultaneously reducing (increasing) the radiation reaching the planet's surface. Overall, we conclude that the update of the AO optical properties is accomplished successfully and confirmed by the evaluation simulations.

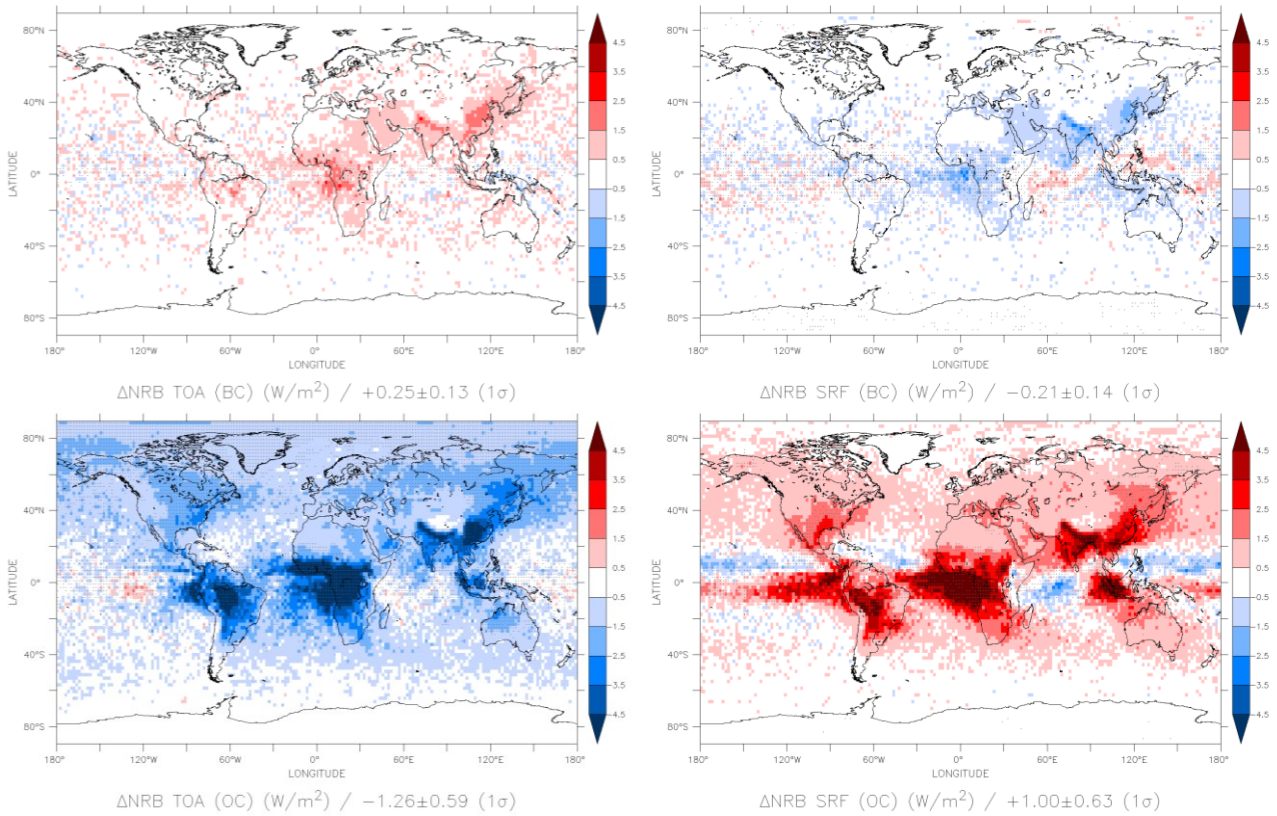

Figure 4. Changes to the instantaneous radiative forcing at the top of atmosphere (left panels) and surface (right panels) due to the updated optical properties of BC (upper panels) and OC (lower panels) in EMAC. Sensitivities are obtained for the 2000–2020 period, stippled areas denote statistically significant differences (Welch *t*-test, two-tailed, α=0.05).

2.2 EC-Earth

EC-Earth is an Earth System Model (ESM) collaboratively developed by a consortium of European meteorological services and research institutes (https://ec-earth.org/; Döscher et al., 2022). At present, the EC-Earth4 version is being developed, which will be the basis for the contribution to the phase 7 of the Coupled Model Intercomparison Project (CMIP7). Within this effort, FOCI has allowed to introduce novelties and improvements in the calculation of the aerosols' optical properties of the model, with a focus on mineral dust.

Dust aerosols have been often simulated in ESMs as compositionally homogeneous entities, neglecting the regional variations in dust composition that arise from the varying mineralogy of source soils (Claquin et al., 1999; Journet et al., 2014). This widely used simplification leads to biases in the global distribution of dust radiation absorption in models (Obiso et al., 2024), because it implies that only size variations determine the absorption variations while the contribution of a varying imaginary refractive index (IRI) is neglected. However, specific minerals such as iron oxides (primarily hematite and goethite) are known to determine the dust absorption at ultraviolet (UV) and visible (VIS) wavelengths (Sokolik and Toon, 1999; Balkanski et al., 2007; Moosmüller et al., 2012). Therefore, at those wavelengths, distinguishing at least two dust components, that is iron oxides and all other weakly-absorbing minerals, represents a first step towards a refined representation of the dust-radiation interaction.

The introduction of varying mineralogy as a factor to the calculation of the dust optical properties requires the representation within the EC-Earth4 framework of the iron oxides as separate tracers, and the introduction of appropriate complex refractive indexes for the iron oxides and the host minerals. The work will be initially conducted in the OpenIFS 48r1 (ECMWF, 2023), the atmospheric core of EC-Earth4, that includes the HAM-M7 aerosol representation (Tegen et al., 2019; Vignati et al., 2004), OIFS48r1-AC from now on.

The introduction of iron oxides as separate tracers will rely in EC-Earth4 in the soil mineralogy map of Claquin et al. (1999), with the modifications of Nickovic et al. (2012). The emitted mineral mass fraction of iron oxides is calculated for the accumulation and coarse modes, where dust is represented, by applying an extension of the brittle fragmentation theory to dust emission (Kok et al., 2011) – see Section 2.2.1

In parallel, the calculation of the appropriate optical properties will be done online by combining the iron oxides complex refractive index with that of the host minerals – see Section 2.2.2.

2.2.1 Emitted mineral fractions of iron oxides

Part of FOCI developments conducted in EC-Earth4 have focused on the implementation of the dust emission scheme of Tegen et al. (2002, 2004). The work done is described in deliverable 3.1 and complemented in deliverable 3.3. Here, we summarize the steps taken to implement the emitted mineral mass fraction for iron oxides to be able to independently trace them in the model.

The information on the soil mineralogy of the arid and semi-arid regions of the world is based on the soil mineralogy atlas of Claquin et al. (1999), with the updates included by Nickovic et al. (2012). The atlas is built relying in literature data of soil descriptions that are used to create a mean mineralogical composition of different soil types, from those defined by the Food and Agriculture Organization of the United Nations (FAO, 1974). Linking these two sources of information it is possible to describe the geographical distribution of mineralogical fractions (%w) for two soil size classes, clay (up to 2 μm) and silt (2 to 63 μm) over the main dust sources at the global scale. The map provides information on 8 minerals relevant for their climatological impacts, amongst them hematite, which is considered in this study as a proxy for the abundance of iron oxides in the soil (i.e., hematite and goethite together).

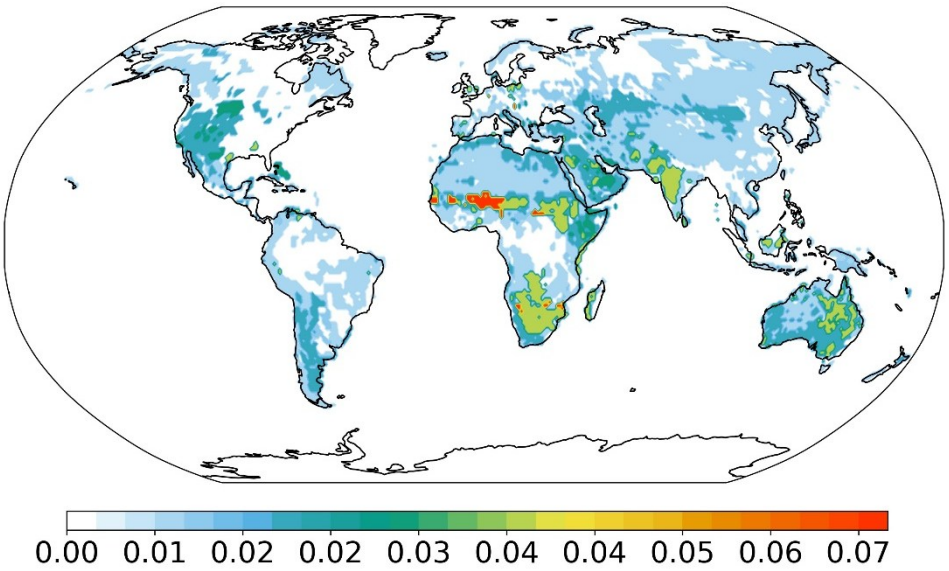

Figure 5. Iron oxides mass fraction at emission as derived from the Claquin et al. 1999; Nickovic et al. 2012 soil maps after the projection in the accumulation and coarse modes of OIFS48r1-AC. The assumption of the underlying soil maps of assigning the same iron oxide relative content across soil particles results in the same mass fraction for both modes, only the accumulation mode is shown.

The mineral mass fraction in the soils differs from that in the airborne dust, particularly because the determination of mineral abundances in soils is usually conducted via destructive techniques (e.g., wet sieving), that break soil aggregates that are many times found in the airborne dust samples. To circumvent this issue, several previous works have applied an extension of the brittle fragmentation theory for dust emission (Perlwitz et al., 2015; Gonçalves Ageitos et al., 2023), that allows reconstructing the emitted particle size distribution of dust relying on information from the disturbed parent soil size distribution (Kok et al., 2011).

In this case, we apply the BFT to derive the mass fraction at emission for the iron oxides in the accumulation and coarse modes, defined for dust, considering the dry mass median diameter (0.74 and 3.5 μm, respectively) and standard deviation (1.59 and 2 μm, respectively) of these modes. We obtain then a %w of iron oxides per grid cell at 1ºx1º resolution at the global scale, that can then be applied to the dust emission flux as estimated by the EC-Earth4 (shown in Figure 5).

2.2.2 Calculation of optical properties.

OIFS48r1-AC uses a modal aerosol representation, M7 (Vignati et al., 2004). Dust is present in the accumulation and coarse modes by its own (insoluble) or internally mixed with other aerosol species (soluble). The model calculates the optical properties of aerosols following the Mie theory for each mode, where the different aerosol refractive indices are mixed proportionally to the volume fraction of the aerosol component.

Here, we supply the model with this new feature adopting a semi-empirical approach that builds upon the methodology developed by Obiso et al. (2024). This approach relies on dust measurements by Di Biagio et al. (2019; DB19 hereafter) to derive new observationally constrained IRIs for iron oxides. This allows us to circumvent the uncertainty of a large range of possible values for hematite available in the literature (Zhang et al., 2015) as well as the lack of measurements for goethite at UV-VIS wavelengths. DB19 re-suspended in a laboratory chamber a number of dust samples collected in different source regions and simultaneously measured the mineral composition and the refractive index of dust aerosols at seven solar wavelengths ranging from 0.370 to 0.950 μm. One of their findings was a quasi-linear relation of the retrieved dust IRI at each wavelength to the

fractional content of iron oxides measured in the samples. We take advantage of this result to derive a new set of IRIs for iron oxides, through an inversion procedure based upon a theoretical particle model.

By retrieving a single IRI for each dust sample using Mie theory, DB19 implicitly assumed that dust particles in their samples were spheres with homogeneous composition across sizes (up to 10 μm in diameter). To derive a separate IRI for iron oxides (including both hematite and goethite), it is necessary to apply a mixing rule for refractive indices. We therefore make the additional assumption that all particles were internal mixtures of a host amalgam (i.e., non-iron oxide minerals blended together) and small inclusions of iron oxides, whose volume fraction was constant in each sample but varying across different samples. This hypothesis is consistent with the Maxwell Garnett mixing rule (Markel, 2016), which gives the effective complex permittivity: $\varepsilon = (n + ik)^2$, with n being the real part of the complex refractive index and k the imaginary part (IRI). starting from the permittivities of a homogeneous host medium and small accretions (iron oxides).

We define the host component by mixing refractive indices of individual weakly-absorbing minerals collected by Scanza et al. (2015), according to global volume fractions of the same minerals calculated by the MONARCH model (Pérez et al., 2011; Gonçalves et al., 2023) featuring mineral speciation of dust based on the soil mineralogy map from Claquin et al. (1999). We then fit a linear model to the relation of dust IRI to the iron oxide fraction found by DB19, at each of their seven experimental wavelengths, imposing the IRI of the host amalgam as the intercept and setting the linear slope as the only free fit parameter. As a final step, we match the experimental slope to a theoretical expression derived by linearizing the Maxwell Garnett rule (Markel, 2016) for small volume fractions of the inclusion (Obiso et al., 2024). Because the IRI of iron oxides is the only unknown (for the real index we use the hematite value from Scanza et al., 2015), this equation allows us to calculate its value by minimizing the difference between theoretical and experimental estimates.

This inversion procedure allows us to estimate the IRI of iron oxides at the seven experimental wavelengths of DB19. We calculate the values at the UV-VIS wavelengths of OIFS48r1-AC by linear interpolation. For wavelengths outside these bands, we use the hematite IRI collected by Scanza et al. (2015). In Table 2, we report the new IRIs for host amalgam and iron oxides at the UV-VIS wavelengths of OIFS48r1-AC, along with the dust IRIs currently used in the model.

Table 2. New imaginary refractive indices (k) for host amalgam and iron oxides (irox), along with the values for dust currently used in EC-Earth4, at the ultraviolet-visible wavelengths (λ) included in the model.

λ (μm)	0.230	0.300	0.390	0.530	0.700
k_{host}	$1.25 \cdot 10^{-3}$	$1.07 \cdot 10^{-3}$	$6.87 \cdot 10^{-4}$	$3.44 \cdot 10^{-4}$	$3.65 \cdot 10^{-4}$
k_{irox}	$1.63 \cdot 10^{-1}$	$1.63 \cdot 10^{-1}$	$1.63 \cdot 10^{-1}$	$1.20 \cdot 10^{-1}$	$4.48 \cdot 10^{-2}$
k_{dust}	$2.50 \cdot 10^{-2}$	$2.00 \cdot 10^{-2}$	$2.50 \cdot 10^{-3}$	$1.00 \cdot 10^{-3}$	$9.50 \cdot 10^{-4}$

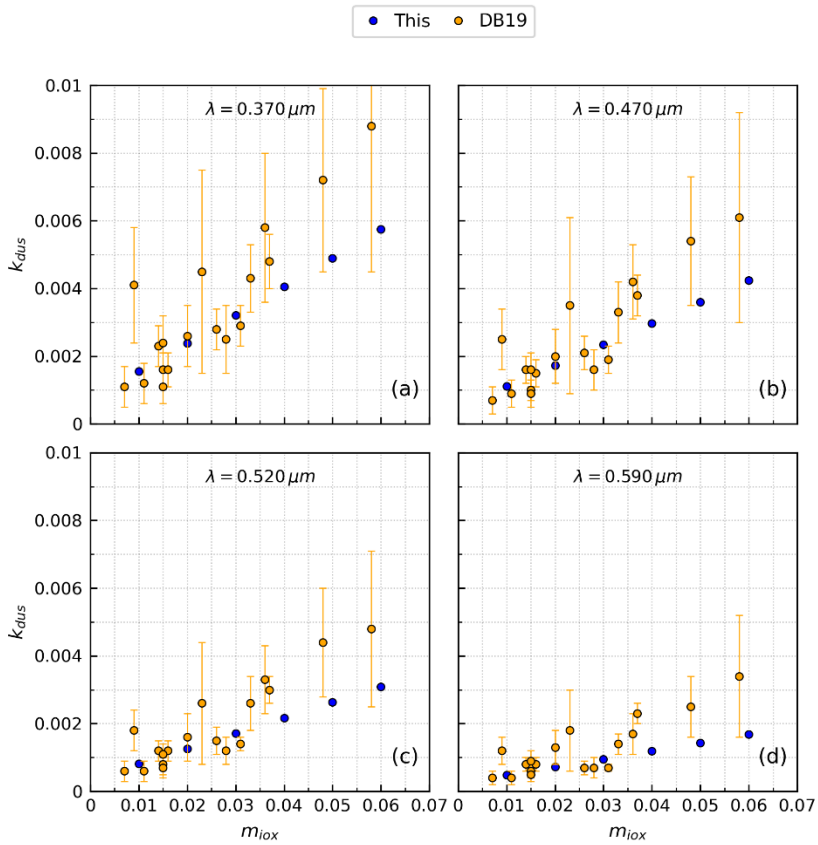

Figure 6. Panels a-d: Comparison between imaginary refractive indices (IRIs) of 18 dust samples from Di Biagio et al. (2019) (orange symbols) and our values (blue symbols) calculated by mixing the IRIs of host amalgam and iron oxides from Table 2, using the Maxwell Garnett mixing rule and assuming mass fractions of iron oxides from 0.01 to 0.06, at the four shortest experimental wavelengths from Di Biagio et al. (2019).

In Figures 6-a to 6-d, we compare the IRIs of a dust mixture composed of the host amalgam and increasing mass fractions of iron oxides (from 0.01 to 0.06), calculated by mixing our IRIs of the two components reported in Table 1 through the Maxwell Garnett rule, with the dust IRIs of 18 samples retrieved by DB19 at their four shortest experimental wavelengths. These plots demonstrate that our newly derived IRIs for iron oxides, and the host IRI as the value in the limit of vanishing iron oxides, explain the empirical relationships between dust IRI and iron oxide content found by DB19. We actually see a stronger agreement for small mass fractions of iron oxides, whereas for larger fractions the calculated IRIs seem to underestimate the experimental data. In this regard, it is worth noting that our calculations are fairly consistent with those experimental data that have a smaller error bar and thus a higher weight in the linear fit.

In Figure 7, we show our new IRIs for iron oxides, at the visible wavelengths of DB19, compared to data sets available in the literature (mostly referring to the sole hematite). Primarily at UV and short-VIS wavelengths, we see that our observationally constrained IRI for iron oxides is much lower than other widely used values (i.e., Querry, 1985; Longtin et al., 1988; Scanza et al., 2015) but consistent with the data from Bedidi and Cervelle (1993), which to our best knowledge is the only study reporting values for goethite at VIS wavelengths. This implies that our inversion of the experimental data of DB19 leads to a weaker absorption of radiation by dust even at those wavelengths where the absorption of iron oxides typically peaks.

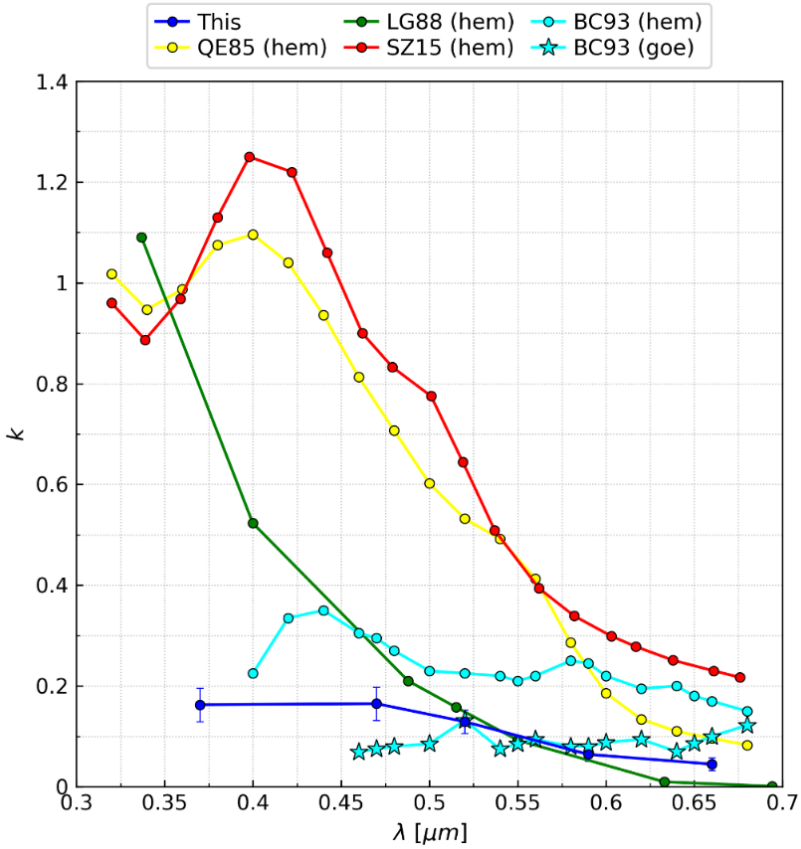

Figure 7. Comparison between our IRIs for iron oxides at the visible wavelengths of Di Biagio et al. (2019) and values from the literature, mostly for hematite; the referenced studies are Querry (1985; QE85), Longtin et al. (1988; LG88), Scanza et al. (2015; SZ15) and Bedidi and Cervelle (1993; BC93).

5. OUTLOOK

We have reported on advancements made in the representation of aerosols optical properties in EC-Earth4 and EMAC. Details on developments related to aerosol-cloud interactions are to be given in the Deliverable D3.3. For EMAC, we have presented the improvements and the implementation of new wavelength dependencies for carbonaceous material, i.e. Black Carbon, Brown Carbon as well as Organic Aerosols (primary and secondary). In the EC-Earth4 model, the wavelength dependence of the imaginary part of the refractive index for dust aerosols have been implemented, depending also on the dust composition. In the coming months a large part of the efforts will be devoted to evaluating the effect of such changes in representing the aerosols optical depth on a global scale and quantifying the improvements in the model representation against observational data. In addition, a more detail evaluation of the model numerical results will be reported in D3.4.

REFERENCES

Alexander, D. T. L., Crozier, P. A., and Anderson, J. R.: Brown carbon spheres in East Asian outflow and their optical properties, Science, 321, 833–836, https://doi.org/10.1126/science.1155296, 2008.

Bohren, C. F. and Huffman, D. R.: Absorption and scattering of light by small particles, 1st ed., Wiley, https://doi.org/10.1002/9783527618156, 1998.

Balkanski, Y., Schulz, M., Claquin, T., and Guibert, S.: Reevaluation of Mineral aerosol radiative forcings suggests a better agreement with satellite and AERONET data, Atmos. Chem. Phys., 7, 81–95, https://doi.org/10.5194/acp-7-81-2007, 2007.

Bedidi, A. and Cervelle, B.: Light scattering by spherical particles with hematite and goethitelike optical properties: Effect of water impregnation, J. Geophys. Res.-Solid Earth, 98, 11941–11952, https://doi.org/10.1029/93JB00188, 1993.

Claquin, T., Schulz, M., and Balkanski, Y. J.: Modeling the mineralogy of atmospheric dust sources, J. Geophys. Res.-Atmos., 104, 22243–22256, https://doi.org/10.1029/1999JD900416, 1999.

Di Biagio, C., Formenti, P., Balkanski, Y., Caponi, L., Cazaunau, M., Pangui, E., Journet, E., Nowak, S., Andreae, M. O., Kandler, K., Saeed, T., Piketh, S., Seibert, D., Williams, E., and Doussin, J.-F.: Complex refractive indices and single-scattering albedo of global dust aerosols in the shortwave spectrum and relationship to size and iron content, Atmos. Chem. Phys., 19, 15503–15531, https://doi.org/10.5194/acp-19-15503-2019, 2019.

Döscher, R., Acosta, M., Alessandri, A., Anthoni, P., Arsouze, T., Bergman, T., Bernardello, R., Boussetta, S., Caron, L.-P., Carver, G., Castrillo, M., Catalano, F., Cvijanovic, I., Davini, P., Dekker, E., Doblas-Reyes, F. J., Docquier, D., Echevarria, P., Fladrich, U., Fuentes-Franco, R., Gröger, M., v. Hardenberg, J., Hieronymus, J., Karami, M. P., Keskinen, J.-P., Koenigk, T., Makkonen, R., Massonnet, F., Ménégoz, M., Miller, P. A., Moreno-Chamarro, E., Nieradzik, L., van Noije, T., Nolan, P., O'Donnell, D., Ollinaho, P., van den Oord, G., Ortega, P., Prims, O. T., Ramos, A., Reerink, T., Rousset, C., Ruprich-Robert, Y., Le Sager, P., Schmith, T., Schrödner, R., Serva, F., Sicardi, V., Sloth Madsen, M., Smith, B., Tian, T., Tourigny, E., Uotila, P., Vancoppenolle, M., Wang, S., Wårlind, D., Willén, U., Wyser, K., Yang, S., Yepes-Arbós, X., and Zhang, Q.: The EC-Earth3 Earth system model for the Coupled Model Intercomparison Project 6, Geosci. Model Dev., 15, 2973–3020, https://doi.org/10.5194/gmd-15-2973-2022, 2022.

ECMWF: IFS Documentation CY48R1 – Part VIII: Atmospheric Composition, ECMWF, pp. 84, https://doi.org/10.21957/749dc09059, 2023.

FAO-UNESCO: Soil Map of the World – Volume I Legend, Food and Agriculture Organization – United Nations Educational Scientific and Cultural Organization, Paris, http://www.fao.org/3/as360e/as360e.pdf (last access: 6 December 2022), 1974.

Gonçalves Ageitos, M., Obiso, V., Miller, R. L., Jorba, O., Klose, M., Dawson, M., Balkanski, Y., Perlwitz, J., Basart, S., Di Tomaso, E., Escribano, J., Macchia, F., Montané, G., Mahowald, N. M., Green, R. O., Thompson, D. R., and Pérez García-Pando, C.: Modeling dust mineralogical composition: sensitivity to soil mineralogy atlases and their expected climate impacts, Atmos. Chem. Phys., 23, 8623–8657, https://doi.org/10.5194/acp-23-8623-2023, 2023.

Gromov, S., Taraborrelli, D., and Pozzer, A.: Sensitivity of organic aerosol optical properties to improved representation of brown carbon in the EMAC model, EGU General Assembly 2024, Vienna, Austria, https://doi.org/10.5194/egusphere-egu24-18402, 2025.

Hoffer, A., Tóth, Á., Pósfai, M., Chung, C. E., and Gelencsér, A.: Brown carbon absorption in the red and near-infrared spectral region, Atmos. Meas. Tech., 10, 2353–2359, https://doi.org/10.5194/amt-10-2353-2017, 2017.

Huang, X., Chen, X., and Yue, Q.: Band-by-band contributions to the longwave cloud radiative feedbacks, Geophys. Res. Lett., 46, 6998–7006, https://doi.org/10.1029/2019GL083466, 2019.

IPCC: Climate change 2021 – the physical science basis: working group I contribution to the sixth assessment report of the intergovernmental panel on climate change, 1st ed., Cambridge University Press, https://doi.org/10.1017/9781009157896, 2023.

Jöckel, P., Sander, R., Kerkweg, A., Tost, H., and Lelieveld, J.: Technical note: the modular earth submodel system (MESSy) – a new approach towards earth system modeling, Atmos. Chem. Phys., 5, 433−444, https://doi.org/10.5194/acp-5-433-2005, 2005.

Jöckel, P., Tost, H., Pozzer, A., Brühl, C., Buchholz, J., Ganzeveld, L., Hoor, P., Kerkweg, A., Lawrence, M. G., Sander, R., Steil, B., Stiller, G., Tanarhte, M., Taraborrelli, D., van Aardenne, J., and Lelieveld, J.: The atmospheric chemistry general circulation model ECHAM5/MESSy1: consistent simulation of ozone from the surface to the mesosphere, Atmos. Chem. Phys., 6, 5067−5104, https://doi.org/10.5194/acp-6-5067-2006, 2006.

Journet, E., Balkanski, Y., and Harrison, S. P.: A new data set of soil mineralogy for dust-cycle modeling, Atmos. Chem. Phys., 14, 3801–3816, https://doi.org/10.5194/acp-14-3801-2014, 2014.

Kok, J. F.: A scaling theory for the size distribution of emitted dust aerosols suggests climate models underestimate the size of the global dust cycle, P. Natl. Sci. USA, 108, 1016–1021, https://doi.org/10.1073/pnas.1014798108, 2011.

Longtin, D. R., Shettle, E. P., Hummel, J. R., and Pryce, J. D.: A wind dependent desert aerosol model: Radiative properties, Tech. Rep. AFGL-TR-88-0112, Air Force Geophysics Laboratory, Hanscom AFB, MA, USA, 114 pp., https://apps.dtic.mil/sti/pdfs/ADA201951.pdf (last access: 3 March 2024), 1988.

Markel, V. A.: Introduction to the Maxwell Garnett approximation: tutorial, J. Opt. Soc. Am. A, 33, 1244–1256, https://doi.org/10.1364/JOSAA.33.001244, 2016.

Moosmüller, H., Engelbrecht, J. P., Skiba, M., Frey, G., Chakrabarty, R. K., and Arnott, W. P.: Single scattering albedo of fine mineral dust aerosols controlled by iron concentration, J. Geophys. Res.-Atmos., 117, D11210, https://doi.org/10.1029/2011JD016909, 2012.

Nickovic, S., Vukovic, A., Vujadinovic, M., Djurdjevic, V., and Pejanovic, G.: Technical Note: High-resolution mineralogical database of dust-productive soils for atmospheric dust modeling, Atmos. Chem. Phys., 12, 845–855, https://doi.org/10.5194/acp-12-845-2012, 2012.

Obiso, V., Gonçalves Ageitos, M., Pérez García-Pando, C., Perlwitz, J. P., Schuster, G. L., Bauer, S. E., Di Biagio, C., Formenti, P., Tsigaridis, K., and Miller, R. L.: Observationally constrained regional variations of shortwave absorption by iron oxides emphasize the cooling effect of dust, Atmos. Chem. Phys., 24, 5337–5367, https://doi.org/10.5194/acp-24-5337-2024, 2024.

Pérez, C., Haustein, K., Janjic, Z., Jorba, O., Huneeus, N., Baldasano, J. M., Black, T., Basart, S., Nickovic, S., Miller, R. L., Perlwitz, J. P., Schulz, M., and Thomson, M.: Atmospheric dust modeling from meso to global scales with the online NMMB/BSC-Dust model – Part 1: Model description, annual simulations and evaluation, Atmos. Chem. Phys., 11, 13001–13027, https://doi.org/10.5194/acp-11-13001-2011, 2011.

Perlwitz, J. P., Pérez García-Pando, C., and Miller, R. L.: Predicting the mineral composition of dust aerosols – Part 1: Representing key processes, Atmos. Chem. Phys., 15, 11593–11627, https://doi.org/10.5194/acp-15-11593-2015, 2015.

Pozzer, A., Reifenberg, S. F., Kumar, V., Franco, B., Kohl, M., Taraborrelli, D., Gromov, S., Ehrhart, S., Jöckel, P., Sander, R., Fall, V., Rosanka, S., Karydis, V., Akritidis, D., Emmerichs, T., Crippa, M., Guizzardi, D., Kaiser, J. W., Clarisse, L., Kiendler-Scharr, A., Tost, H., and Tsimpidi, A.: Simulation of organics in the atmosphere: evaluation of EMACv2.54 with the Mainz organic mechanism (MOM) coupled to the ORACLE (v1.0) submodel, Geosci. Model Dev., 15, 2673–2710, https://doi.org/10.5194/gmd-15-2673-2022, 2022.

Querry, M. R.: Optical constants, Tech. Rep. CRDC-CR-85034, University of Missouri, Kansas City, MO, USA, 413 pp., https://apps.dtic.mil/sti/pdfs/ADA158623.pdf (last access: 3 March 2024), 1985.

Roeckner, E., Brokopf, R., Esch, M., Giorgetta, M., Hagemann, S., Kornblueh, L., Manzini, E., Schlese, U., and Schulzweida, U.: Sensitivity of simulated climate to horizontal and vertical resolution in the ECHAM5 atmosphere model, J. Clim., 19, 3771−3791, https://doi.org/10.1175/JCLI3824.1, 2006.

Schallock, J., Brühl, C., Bingen, C., Höpfner, M., Rieger, L., and Lelieveld, J.: Reconstructing volcanic radiative forcing since 1990, using a comprehensive emission inventory and spatially resolved sulfur injections from satellite data in a chemistry-climate model, Atmos. Chem. Phys., 23, 1169–1207, https://doi.org/10.5194/acp-23-1169-2023, 2023.

Scanza, R. A., Mahowald, N., Ghan, S., Zender, C. S., Kok, J. F., Liu, X., Zhang, Y., and Albani, S.: Modeling dust as component minerals in the Community Atmosphere Model: development of framework and impact on radiative forcing, Atmos. Chem. Phys., 15, 537–561, https://doi.org/10.5194/acp-15-537-2015, 2015.

Sokolik, I. N. and Toon, O. B.: Incorporation of mineralogical composition into models of the radiative properties of mineral aerosol from UV to IR wavelengths, J. Geophys. Res.-Atmos., 104, 9423–9444, https://doi.org/10.1029/1998JD200048, 1999.

Tegen, I., Harrison, S. P., Kohfeld, K., Prentice, I. C., Coe, M., and Heimann, M.: Impact of vegetation and preferential source areas on global dust aerosol: Results from a model study, J. Geophys. Res., 107(D21), 4576, https://doi.org/10.1029/2001JD000963, 2002.

Tegen, I., Werner, M., Harrison, S. P., and Kohfeld, K. E.: Relative importance of climate and land use in determining present and future global soil dust emission, Geophys. Res. Lett., 31, L05105, https://doi.org/10.1029/2003GL019216, 2004.

Tegen, I., Neubauer, D., Ferrachat, S., Siegenthaler-Le Drian, C., Bey, I., Schutgens, N., Stier, P., Watson-Parris, D., Stanelle, T., Schmidt, H., Rast, S., Kokkola, H., Schultz, M., Schroeder, S., Daskalakis, N., Barthel, S., Heinold, B., and Lohmann, U.: The global aerosol–climate model ECHAM6.3–HAM2.3 – Part 1: Aerosol evaluation, Geosci. Model Dev., 12, 1643–1677, https://doi.org/10.5194/gmd-12-1643-2019, 2019.

Vignati, E., Wilson, J., and Stier, P.: M7: An efficient size-resolved aerosol microphysics module for large-scale aerosol transport models, J. Geophys. Res., 109, D22202, https://doi.org/10.1029/2003JD004485, 2004.

Vignati, E., Wilson, J., and Stier, P.: M7: An efficient size-resolved aerosol microphysics module for large-scale aerosol transport models, J. Geophys. Res., 109, D22202, https://doi.org/10.1029/2003JD004485, 2004.

Zhang, X. L., Wu, G. J., Zhang, C. L., Xu, T. L., and Zhou, Q. Q.: What is the real role of iron oxides in the optical properties of dust aerosols?, Atmos. Chem. Phys., 15, 12159–12177, https://doi.org/10.5194/acp-15-12159-2015, 2015.